entropy

MDPI

Article

Entropy Generation Analysis of Hybrid Nanomaterial through Porous Space with Variable Characteristics

Muhammad Adil Sadiq [1,*], Farwa Haider [2] and Tasawar Hayat [2]

[1] Department of Mathematics, DCC-KFUPM, Dhahran 31261, Saudi Arabia
[2] Department of Mathematics Quaid-I-Azam University, Islamabad 45320, Pakistan; farwahaider3@gmail.com (F.H.); fmgpak@gmail.com (T.H.)
* Correspondence: adilsadiq@kfupm.edu.sa; Tel.: +966-59-865-8229

Abstract: Salient features of hybrid nanofluid (MoS_2-SiO_2/water) for Darcy–Forchheimer–Brinkman porous space with variable characteristics is examined. Heat transfer analysis subject to viscous dissipation, nonlinear thermal radiation, and heat generation/absorption is carried out. Disturbance inflow is created by an exponentially stretching curved sheet. Relevant equations are simplified by employing boundary layer theory. Adequate transformations lead to a set of dimensionless equations. Velocity, temperature, and entropy generation rate are analyzed graphically. Comparative results are obtained for hybrid (MoS_2-SiO_2/water) and nanofluid (MoS_2-water and SiO_2-water). Physical quantities are analyzed through numerical data.

Keywords: hybrid nanofluid (MoS_2 and SiO_2); Darcy–Forchheimer–Brinkman porous space; non-linear thermal radiation; viscous dissipation; heat generation/absorption; ND Solve

Citation: Sadiq, M.A.; Haider, F.; Hayat, T. Entropy Generation Analysis of Hybrid Nanomaterial through Porous Space with Variable Characteristics. *Entropy* **2021**, *23*, 89. https://doi.org/10.3390/e23010089

Received: 17 November 2020
Accepted: 7 January 2021
Published: 10 January 2021

1. Introduction

Electronics, automotive, telecommunication, aerospace, and biomedical industries require microdevices for heat transfer enhancement in a system. Heat transfer efficiency of such devices can be improved by using a working fluid with enhanced thermophysical properties like thermal conductivity and specific heat. Hybrid nanofluids are potential materials produced by dispersing two dissimilar nanoparticles (metals, carbide and oxide ceramics, carbon nanotubes, and metals) in base fluid (ethylene glycol, oil, and water). Such fluids have superior thermophysical properties and thermal performance than nanofluids. Such nanofluids save energy as well as less harmful environmental impacts. After the pioneering work of Choi [1] on nanofluids, several studies have been conducted to analyze the behavior of such materials. Few of these are mentioned here which considered different nanoparticles such as Cu, Al_2O_3, Ag, CuO, and several others. Eastman et al. [2] analyzed improvement in thermal conductivity of ethylene glycol-based copper nanofluid. It is noted that ethylene-glycol based copper nanofluid has much higher effective thermal conductivity than pure ethylene glycol. The flow of nanofluid in a lid-driven square cavity is provided by Tiwari and Das [3] They analyzed the behavior of nanofluid by considering solid volume fraction of nanoparticles. Vajravelu et al. [4] presented convective heat transfer in Ag-water and Cu-water nanofluids. A comparative analysis is performed for Ag-water and Cu-water nanofluids. It is observed that boundary layer thickness decreases more rapidly in the case of Ag-water nanofluid in comparison to Cu-water. The three-dimensional flow of nanofluid is examined by Khan et al. [5]. Devasenan and Kalaiselvam [6] provided an experimental investigation of the heat transfer behavior of hybrid nanofluid. Copper-titanium hybrid nanocomposites are considered. They found an increase in thermal conductivity due to the highly crystalline nature of copper-titanium hybrid nanofluid. Malvandi et al. [7] discussed mixed convection in Al_2O_3-water nanofluid. Selimefendigil et al. [8] elaborated mixed convection in SiO_2-water nanofluid by a rotating cylinder. Different shapes of nanoparticles are considered such as spherical, cylindrical, brick, and blade. It is analyzed

that the heat transfer rate of cylindrically shaped nanoparticles is higher than that of others. Improvement in heat transfer of Ag-CuO/water nanofluid is addressed by Hayat and Nadeem [9]. Iqbal et al. [10] analyzed curvilinear transport of MoS_2-SiO_2/water nanofluid. It is noted that blade-shaped nanoparticles have maximum temperature while brick-shaped nanoparticles have the lowest temperature. Thermally radiative flow of Cu-Al_2O_3/water nanomaterial over a permeable surface is interpreted by Usman et al. [11] Mansour et al. [12] provided entropy generation analysis of square porous cavity filled with Al_2O_3-Cu/water nanofluid. The influence of internal heat generation in the flow of MoS_2-SiO_2/$C_3H_8O_2$ is studied by Shaiq et al. [13] Khan et al. [14] analyzed entropy generation analysis of MoS_2-SiO_2/$C_3H_8O_2$ nanofluid with variable viscosity. Heat transfer enhancement in hybrid nanofluid along the wavy surface is studied by Iqbal et al. [15]. It is noted that hybrid nanofluid has a higher transfer rate than nanomaterial. Khan et al. [16] presented an entropy generation analysis of MoS_2-SiO_2/ water nanofluid through porous space. Acharya [17] analyzed the behavior of hybrid nanofluid inside a microchannel. Hydromagnetic flow of Cu-Al_2O_3/water nanofluid past moving sheet is illustrated by Aladdin et al. [18] Flow of hybrid nanofluid saturating porous medium with mixed convection is discussed by Waini et al. [19] Aly and Pop [20] provided comparative analysis for stagnation point flow of hybrid nanofluid and nanomaterial with MHD.

Porous space is composed of interconnected solid particles and pores generally encountered in electrochemical systems, iron and steel making, microchemical reactors, biofiltration systems, and combustion of carbon-neutral and renewable fuels. Extensive theoretical and computational studies about porous media are based on classical Darcy's law. To include inertia and viscous diffusion effects in Darcy's law, the modifications are made by Forchheimer [21] and Brinkman [22,23] respectively. To resolve this paradox, Nield [24] modeled viscous dissipation in a porous medium. Hadhrami et al. [25] provided another model for viscous dissipation in porous space. Mixed convective flow through porous space is analyzed by Seddeek [26] Umavathi et al. [27] illustrated Darcy-Forchheimer-Brinkman flow of nanofluid in a vertical rectangular duct. Latest developments in flow through a porous medium with constant porosity and permeability and can be cited through refs. [28–36]. However little information is available for variable characteristics of porous space [37–44]

Entropy generation is a quantitative tool based on the second law of thermodynamics. It measures irreversibilities in the fluid flow process. Heat and mass transfer, viscous dissipation, buoyancy, and magnetic field are the source of chaos in a thermal system. Several studies are conducted to anticipate the entropy generation rate in thermal systems followed by the pioneering work of Bejan [45]. Entropy generation of nanofluid in a cavity is analyzed by Mahmoudi et al. [46]. It is observed that the entropy generation rate decreases due to the addition of nanoparticles. Entropy generation analysis of nanofluid in a vertical porous microchannel is provided by López et al. [47] Sithole et al. [48] explored entropy generation analysis of nanofluid with nonlinear thermal radiation. It is noted that the entropy generation rate decreases in presence of thermal radiation. Entropy generation analysis of ferrofluid saturating porous space is elaborated by Astanina et al. [49]. Huminic and Huminic [50] discussed entropy generation analysis of hybrid nanofluid. Entropy generation analysis of viscous fluid with buoyancy is interpreted by Ganesh et al. [51] Kashyap and Dass [52] deliberated entropy generation analysis of the two-phase mixed convective flow of hybrid nanofluid. The effects of three different boundary conditions on fluid flow are analyzed. It is observed that the entropy generation rate increases by a change in the boundary condition. Moreover, the addition of nanoparticles also augments the entropy generation rate which is not desirable for the effectiveness of a thermal system. Entropy generation for nanofluid through non-Darcy porous space is studied by Sheikholeslami et al. [53] Effect of activation energy inflow over the curved surface with entropy generation is analyzed by Muhammad et al. [54] Hayat et al. [55] provided entropy generation for the flow of nanofluid due to curved surface filling porous space. Hayat et al. [56] presented entropy generation analysis of effective Prandtl number.

In view of the above-mentioned studies, the main objectives of the present study are threefold. Firstly, to formulate the flow of hybrid nanofluid by a curved stretching surface through porous space. Variable porosity and permeability are chosen. This concept is given a little attention even for flow by flat stretching case. Secondly, to consider the effects of nonlinear thermal radiation and heat generation/absorption in heat transfer analysis. Thirdly to anticipate the entropy generation rate in the considered problem. Solution development is due to the NDSolve technique of Mathematica. Characteristics of flow, thermal field, and entropy generation rate through involved variables are interpreted. Numerical computations are obtained for physical quantities.

2. Model Development

Here the flow of hybrid nanofluid through Darcy–Forchheimer–Brinkman porous space is analyzed. Viscous dissipation, heat generation/absorption, and non-linear thermal radiation are also taken. The disturbance in flow is created by a curved stretching surface. The sheet is stretched with an exponential velocity $u_w(s) = ae^{s/L}$ (see Figure 1). Here curvilinear coordinates frame (s, r) is adopted. Relevant equations for the considered problem are

$$\frac{\partial}{\partial r}((r+R)v) + R\frac{\partial u}{\partial s} = 0, \tag{1}$$

$$\frac{u^2}{r+R} = \frac{1}{\rho_{hnf}}\frac{\partial p}{\partial r}, \tag{2}$$

$$\begin{aligned} &v\tfrac{\partial u}{\partial r} + \tfrac{R}{r+R}u\tfrac{\partial u}{\partial s} + \tfrac{uv}{r+R} = -\tfrac{1}{\rho_{hnf}}\tfrac{R}{r+R}\tfrac{\partial p}{\partial s} + \\ &\nu_{hnf}\left(\tfrac{\partial^2 u}{\partial r^2} + \tfrac{1}{r+R}\tfrac{\partial u}{\partial r} - \tfrac{u}{(r+R)^2}\right) - \nu_{hnf}\tfrac{\varepsilon(r)}{k^*(r)}u - \tfrac{C_b\varepsilon^2(r)}{(k^*(r))^{1/2}}u^2, \end{aligned} \tag{3}$$

$$\begin{aligned} v\frac{\partial T}{\partial r} + u\frac{\partial T}{\partial s}\frac{R}{r+R} =& \alpha_{hnf}\left(\frac{\partial^2 T}{\partial r^2} + \frac{1}{r+R}\frac{\partial T}{\partial r}\right) + \frac{\mu_{hnf}}{(\rho c_p)_{hnf}}\left(\frac{\partial u}{\partial r} - \frac{u}{r+R}\right)^2 + \\ &\frac{Q}{(\rho c_p)_{hnf}}(T - T_\infty) - \frac{1}{(\rho c_p)_{hnf}}\frac{\partial}{\partial r}\left(-\frac{16\widetilde{\sigma}}{3k}T^3\frac{\partial T}{\partial r}\right) + \frac{\mu_{hnf}}{(\rho c_p)_{hnf}}\frac{\varepsilon(r)}{k^*(r)}u^2 + \\ &\frac{\rho_{hnf}}{(\rho c_p)_{hnf}}\frac{C_b\varepsilon^2(r)}{(k^*(r))^{1/2}}u^3, \end{aligned} \tag{4}$$

$$u = ae^{s/L},\ v = 0,\ T = T_f = T_\infty + T_0e^{As/2L} \text{ at } r = 0, \tag{5}$$

$$u \to 0,\ \frac{\partial u}{\partial r} \to 0,\ T \to T_\infty \text{ as } r \to \infty, \tag{6}$$

where

$$k^*(r) = k_\infty\left(1 + de^{-\frac{r}{\gamma}}\right), \tag{7}$$

$$\varepsilon(r) = \varepsilon_\infty\left(1 + d^*e^{-\frac{r}{\gamma}}\right). \tag{8}$$

Model for hybrid nanofluid is [13]:

$$\begin{aligned} &\mu_{hnf} = \tfrac{\mu_f}{(1-\phi_1-\phi_2)^{2.5}},\ \nu_{hnf} = \tfrac{\mu_{hnf}}{\rho_{hnf}},\ \rho_{hnf} = \rho_f(1-\phi_1-\phi_2) + \rho_1\phi_1 + \rho_2\phi_2, \\ &\alpha_{hnf} = \tfrac{k_{hnf}}{(\rho c_p)_{hnf}},\ (\rho c_p)_{hnf} = (\rho c_p)_f(1-\phi_1-\phi_2) + (\rho c_p)_1\phi_1 + (\rho c_p)_1\phi_1, \\ &\tfrac{k_{hnf}}{k_f} = \tfrac{\phi_1k_1+\phi_2k_2+2\phi k_f+2\phi(\phi_1k_1+\phi_2k_2)-2(\phi_1+\phi_2)^2k_f}{\phi_1k_1+\phi_2k_2+2\phi k_f-\phi(\phi_1k_1+\phi_2k_2)+(\phi_1+\phi_2)^2k_f}. \end{aligned} \tag{9}$$

Here ϕ_1 signifies solid volume fraction of SiO_2, ϕ_2 the solid volume fraction of MoS_2, ρ_{hnf} hybrid nanofluid density, $(\rho c_p)_{hnf}$ heat capacity of hybrid nanofluid, μ_{hnf} effective dynamic viscosity of hybrid nanofluid, k_{hnf} the thermal conductivity of hybrid nanofluid, ρ_1 the density of SiO_2, ρ_2 the density of MoS_2, k_1 the thermal conductivity of SiO_2, k_2 the

thermal conductivity of MoS_2, k_f the thermal conductivity of base fluid, ρ_f the density of base fluid, k_∞ and ε_∞ the constant permeability and porosity, d and d^* the variable permeability and porosity, Q the heat generation/absorption, C_b the drag coefficient, $\widetilde{\sigma}$ the Stefan Boltzmann coefficient and k the mean absorption coefficient. Following Table 1 [14] consists of characteristics of base liquids and nanoparticles.

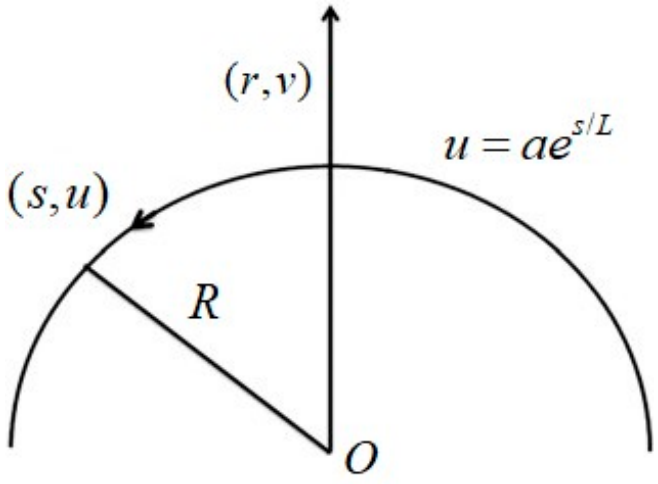

Figure 1. Physical model of flow configuration.

Table 1. Physical properties of base and nanoparticles.

Physical Properties	Base Fluid	Nanoparticles	
	H_2O	SiO_2	MoS_2
ρ (kg/m^3)	997.1	2650	5060
k (W/mK)	0.613	1.5	34.5
C_p (J/kgK)	4179	730	397.746

Considering

$$u = U_w = ae^{s/L}f'(\zeta),\ v = -\frac{R}{r+R}\sqrt{\frac{a\nu_f e^{s/L}}{2L}}(f(\zeta)+\zeta f'(\zeta)),\ \zeta = \left(\frac{ae^{s/L}}{2\nu_f L}\right)^{1/2} r,$$
$$T = T_\infty + T_0 e^{\frac{As}{2L}}\theta(\zeta),\ p = \rho_f a^2 e^{2s/L}H(\zeta), \tag{10}$$

we have

$$\frac{1}{\left(1-\phi_1-\phi_2+\frac{\rho_1}{\rho_f}\phi_1+\frac{\rho_2}{\rho_f}\phi_2\right)}H' = \frac{1}{\zeta+K}f'^2, \tag{11}$$

$$\frac{1}{(1-\phi_1-\phi_2)^{2.5}\left(1-\phi_1-\phi_2+\frac{\rho_1}{\rho_f}\phi_1+\frac{\rho_2}{\rho_f}\phi_2\right)}\left(f''' + \frac{1}{\zeta+K}f'' - \frac{1}{(\zeta+K)^2}f' - 2\frac{1}{\sigma \mathrm{Re}_s}\frac{1+d^*e^{-\zeta}}{1+de^{-\zeta}}f'\right) - \frac{\zeta+2K}{(\zeta+K)^2}K(f')^2 + \frac{K}{\zeta+K}ff'' + \frac{K}{(\zeta+K)^2}ff' - 2\beta\frac{\left(1+d^*e^{-\zeta}\right)^2}{\sqrt{1+de^{-\zeta}}}f'^2 = -\frac{1}{\left(1-\phi_1-\phi_2+\frac{\rho_1}{\rho_f}\phi_1+\frac{\rho_2}{\rho_f}\phi_2\right)}\frac{K}{\zeta+K}(4H+\zeta H') \tag{12}$$

$$\frac{1}{\Pr}\frac{1}{\left(1-\phi_1-\phi_2+\frac{(\rho c_p)_1}{(\rho c_p)_f}\phi_1+\frac{(\rho c_p)_2}{(\rho c_p)_f}\phi_2\right)}\frac{k_{hnf}}{k_f}\left(\theta''+\frac{1}{\zeta+K}\theta'\right)+\frac{K}{\zeta+K}(f\theta'-Af'\theta)+$$
$$\frac{1}{\left(1-\phi_1-\phi_2+\frac{(\rho c_p)_1}{(\rho c_p)_f}\phi_1+\frac{(\rho c_p)_2}{(\rho c_p)_f}\phi_2\right)}\left(2Q^*\theta+\frac{Ec}{(1-\phi_1-\phi_2)^{2.5}}\left(\left(f''-\frac{1}{\zeta+K}f'\right)^2+\frac{2}{\sigma\mathrm{Re}_s}\frac{1+d^*e-\zeta}{1+de^{\zeta}}f'^2\right)-\right. \tag{13}$$
$$\left.\frac{4}{3}\frac{Rd}{\Pr}\left(\left((1+(\theta_w-1)\theta)^3\right)\theta'\right)'+2\frac{\beta Ec}{\left(1-\phi_1-\phi_2+\frac{(\rho c_p)_1}{(\rho c_p)_f}\phi_1+\frac{(\rho c_p)_2}{(\rho c_p)_f}\phi_2\right)}\frac{\left(1+d^*e^{-\zeta}\right)^2}{\sqrt{1+de^{-\zeta}}}f'^3\right)=0,$$

$$f=0,\ f'=1,\ \theta=1 \text{ at } \zeta=0, \tag{14}$$

$$f'\to 0,\ f''\to 0,\ \theta\to 0 \text{ as } \zeta\to\infty. \tag{15}$$

Here Equation (1) is trivially verified. Eliminating pressure H from Equations (11) and (12), we have

$$\frac{1}{(1-\phi_1-\phi_2)^{2.5}\left(1-\phi_1-\phi_2+\frac{\rho_1}{\rho_f}\phi_1+\frac{\rho_2}{\rho_f}\phi_2\right)}\left(f^{iv}+\frac{2}{\zeta+K}f'''-\frac{1}{(\zeta+K)^2}f''+\frac{1}{(\zeta+K)^3}f'-\right.$$
$$\left.2\frac{1}{\sigma\mathrm{Re}_s}\frac{1+d^*e^{-\zeta}}{1+de^{-\zeta}}\left(f''+\frac{1}{\zeta+K}f'\right)\right)+\frac{K}{(\zeta+K)^2}ff''+\frac{K}{\zeta+K}ff'''-\frac{K}{(\zeta+K)^3}ff'- \tag{16}$$
$$\frac{3K}{(\zeta+K)^2}f'^2-\frac{3K}{\zeta+K}f'f''-2\beta\frac{\left(1+d^*e^{-\zeta}\right)^2}{\sqrt{1+de^{-\zeta}}}\left(2f'f''+\frac{1}{\zeta+K}f'^2\right)=0.$$

Here Pe_s depicts the Peclet number, γ the parameter, Re_s the local Reynolds number, β the inertia coefficient, Ec the Eckert number, K the curvature parameter, σ the permeability parameter, Rd the radiation parameter, Q^* the heat generation/absorption parameter, Pr the Prandtl number, and Br the Brinkman number. These definitions are

$$Pe_s=\mathrm{Re}_s\mathrm{Pr},\ \gamma=\sqrt{\frac{\alpha_f}{L}}\frac{Pe_s^{1/2}}{\sqrt{2\nu_f L}},\ \mathrm{Re}_s=\frac{u_w L}{\nu_f},\ \sigma=\frac{k_\infty}{L^2\varepsilon_\infty},\ K=\left(\frac{ae^{s/L}}{2\nu_f L}\right)^{1/2}R,$$
$$\beta=\frac{C_b\varepsilon_\infty^2 L}{\sqrt{k_\infty}},\ Rd=\frac{4\sigma T_\infty^3}{k^*k_f},\ \theta_w=\frac{T_w}{T_\infty},\ Q^*=\frac{QL}{u_w\left(\rho c_p\right)_f},\ Ec=\frac{u_w^2}{(T_w-T_\infty)\left(c_p\right)_f}, \tag{17}$$
$$\Pr=\frac{\nu_f}{\alpha_f},\ Br=\Pr Ec.$$

3. Physical Quantities

Skin friction coefficient and local Nusselt number are given by

$$\left(\frac{\mathrm{Re}_s}{2}\right)^{1/2}C_f=\frac{1}{(1-\phi_1-\phi_2)^{2.5}}\left(f''(0)-\frac{1}{K}f'(0)\right), \tag{18}$$

$$\left(\frac{\mathrm{Re}_s}{2}\right)^{-1/2}Nu_s=-\left(\frac{k_{hnf}}{k_f}+\frac{4}{3}\theta_w^3 Rd\right)\theta'(0). \tag{19}$$

4. Entropy Generation

Entropy generation expression for considered flow problem is

$$S'''_{gen}=\underbrace{\frac{k_{hnf}}{T_m^2}\left(\frac{\partial T}{\partial r}\right)^2}_{\text{Thermal irreversibility}}+\underbrace{\frac{\mu_{hnf}}{T_m}\left(\frac{\partial u}{\partial r}-\frac{u}{r+R}\right)^2}_{\text{Viscous dissipation irreversibility}}+\underbrace{\frac{Q}{T_m}(T-T_\infty)}_{\text{Heat generation/absorption irreversibility}}+$$
$$\underbrace{\frac{1}{T_m}\frac{\partial}{\partial r}\left(-\frac{16\sigma}{3k}T^3\frac{\partial T}{\partial r}\right)}_{\text{Thermal radiation irreversibility}}+\underbrace{\frac{\mu_{hnf}}{T_m}\frac{\varepsilon(r)}{k^*(r)}u^2+\frac{C_b\varepsilon^2(r)\,\rho_{hnf}}{T_m k^{*1/2}}u^3}_{\text{Porous dissipation irreversibility}}, \tag{20}$$

Applying transformations (10) above expression reduces to

$$N_g(\zeta) = \frac{k_{hnf}}{k_f}\alpha_1\theta'^2 + 2\mathrm{Pr}Q^*\theta + \frac{4}{3}Rd\left((1+(\theta_w-1)\theta)^3\theta'\right)' + \frac{Br}{(1-\phi_1-\phi_2)^{2.5}}\left(\left(f'' - \frac{1}{\zeta+K}f'\right)^2 + \frac{2}{\sigma \mathrm{Re}_s}\frac{1+d^*e-\zeta}{1+de^{\zeta}}f'^2\right) + 2\beta Br\left(1-\phi_1-\phi_2+\frac{\rho_1}{\rho_f}\phi_1+\frac{\rho_2}{\rho_f}\phi_2\right)\frac{\left(1+d^*e^{-\zeta}\right)^2}{\sqrt{1+de^{-\zeta}}}f'^3, \quad (21)$$

in which $\alpha_1 = \frac{\Delta T}{T_m}$ is the temperature difference parameter and $N_g = \frac{T_m}{\Delta T}S'''_{gen}\frac{2\nu_f L}{ae^{s/L}}$ the entropy generation rate.

5. Discussion

This section interprets the characteristics of velocity $f'(\zeta)$, temperature $\theta(\zeta)$ and entropy generation rate $N_g(\zeta)$ through curvature parameter (K), porosity parameter (σ), Reynolds number (Re_s), variable porosity and permeability parameters (d) and (d^*), inertia coefficient (β), Brinkman number (Br), temperature exponent (A), temperature ratio parameter (θ_w), radiation parameter (Rd), and heat generation/absorption parameter (Q^*). Comparative results are obtained for hybrid nanofluid (MoS_2-SiO_2/water) and nanofluid (MoS_2/water and SiO_2/ water). The consequences of $f'(\zeta)$ against (K) are in Figure 2. An enhancement in $f'(\zeta)$ is observed through (K) for both hybrid nanofluid and nanomaterial. Physically the bend of the curved stretching sheet contributes in accelerating the flow. The impact of (σ) on $f'(\zeta)$ is illustrated in Figure 3. Here $f'(\zeta)$ is an increasing function of (σ) for both hybrid nanofluid and nanofluid. Velocity $f'(\zeta)$ through (Re_s) is drawn in Figure 4. Higher (Re_s) correspond to stronger $f'(\zeta)$ for both hybrid nanofluid and nanofluid. Physically (Re_s) has a direct relation with inertial forces due to which the velocity increases. Reverse trend of $f'(\zeta)$ is noted for (d) and (d^*) in both hybrid nanofluid and nanofluid (see Figures 5 and 6). Figure 7 is plotted for the features of $f'(\zeta)$ through (β). Higher estimation of (β) lead to a reduction in $f'(\zeta)$ for both hybrid nanofluid (MoS_2-SiO_2/water) and nanofluid (MoS_2/water and SiO_2/water). Figure 8 addressed $\theta(\zeta)$ against (K). By increasing (K) reduction is observed through (K) for both hybrid nanofluid and nanofluid. Figure 9 captured consequences of $\theta(\zeta)$ against (σ). Here reduction in $\theta(\zeta)$ is analyzed through higher (σ) for both hybrid nanofluid and nanofluid. Figure 10 depicts that $\theta(\zeta)$ is a decreasing function of (Re_s) for both hybrid nanofluid (MoS_2-SiO_2/water) and nanofluid (MoS_2/water and SiO_2/ water). Behaviors of $\theta(\zeta)$ through (d) and (d^*) is portrayed in Figures 11 and 12. An enhancement in $\theta(\zeta)$ is observed through (d^*) while opposite trend is seen against (d) for both hybrid nanofluid and nanofluid. Aspects of $\theta(\zeta)$ against (β) is deliberated in Figure 13. Higher (β) produces resilience in the fluid motion due to which more heat is produced which strengthens the thermal field $\theta(\zeta)$ for both hybrid nanofluid (MoS_2-SiO_2/water) and nanofluid (MoS_2/water and SiO_2/ water). Figure 14 cleared that $\theta(\zeta)$ is an increasing function of (Br) for both hybrid nanofluid and nanofluid. Physically (Br) has a direct relation with heat generation by fluid friction which causes stronger $\theta(\zeta)$. Significant behavior of $\theta(\zeta)$ through (A) is drawn in Figure 15. Higher (A) produces weaker $\theta(\zeta)$ in both hybrid nanofluid and nanofluid. Curves of $\theta(\zeta)$ against (Rd) is elucidated in Figure 16. Higher estimation of (Rd) strengthen $\theta(\zeta)$ and more related layer thickness for both hybrid nanofluid and nanofluid. Variation of $\theta(\zeta)$ through (θ_w) is displayed in Figure 17. It is seen that higher (θ_w) enhance $\theta(\zeta)$ for both hybrid nanofluid (MoS_2-SiO_2/water) and nanofluid (MoS_2/water and SiO_2/ water). Role of (Q^*) on $\theta(\zeta)$ is highlighted in Figure 18. Here an augmentation in $\theta(\zeta)$ is observed through (Q^*) for both hybrid nanofluid and nanofluid. Influence of (K) on $N_g(\zeta)$ is depicted in Figure 19. Entropy generation rate decreases due to higher (K) for both hybrid nanofluid and nanofluid. Figures 20 and 21 analyzed the behavior of $N_g(\zeta)$ against (Br) and (Rd). Similar trend of $N_g(\zeta)$ is witnessed through (Br) and (Rd) for both hybrid nanofluid and nanomaterial. Figure 22 illustrates that $N_g(\zeta)$ increases for higher (θ_w) for both hybrid nanofluid (MoS_2-SiO_2/water) and nanofluid (MoS_2/water and SiO_2/water). Impact of

(Q^*) on $N_g(\zeta)$ is sketched in Figure 23. Higher (Q^*) produces augmentation in $\theta(\zeta)$ due to rise in surface temperature for both hybrid nanofluid and nanofluid. Consequences of (α_1) on $N_g(\zeta)$ is highlighted in Figure 24. Here $N_g(\zeta)$ is an increasing function of (α_1) for both hybrid nanofluid and nanofluid. Contribution of involved variables on skin friction coefficient $\left(\frac{\mathrm{Re}_s}{2}\right)^{1/2} C_f$ is displayed in Table 2 Reduction in $\left(\frac{\mathrm{Re}_s}{2}\right)^{1/2} C_f$ is seen through (K), (σ), (Re_s), (d) and (β) for both hybrid nanofluid and nanofluid. Significant behavior of $\left(\frac{\mathrm{Re}_s}{2}\right)^{-1/2} Nu_s$ through influential variables is shown in Table 3 Here (K), (σ), (d), (R_d) and (θ_w) strengthen the $\left(\frac{\mathrm{Re}_s}{2}\right)^{-1/2} Nu_s$ for both hybrid nanofluid and nanofluid. Table 4 is drawn to compare the values of skin friction coefficient with Okechi et al. [28]. It is analyzed that present results are in good agreement with those presented in ref. [28].

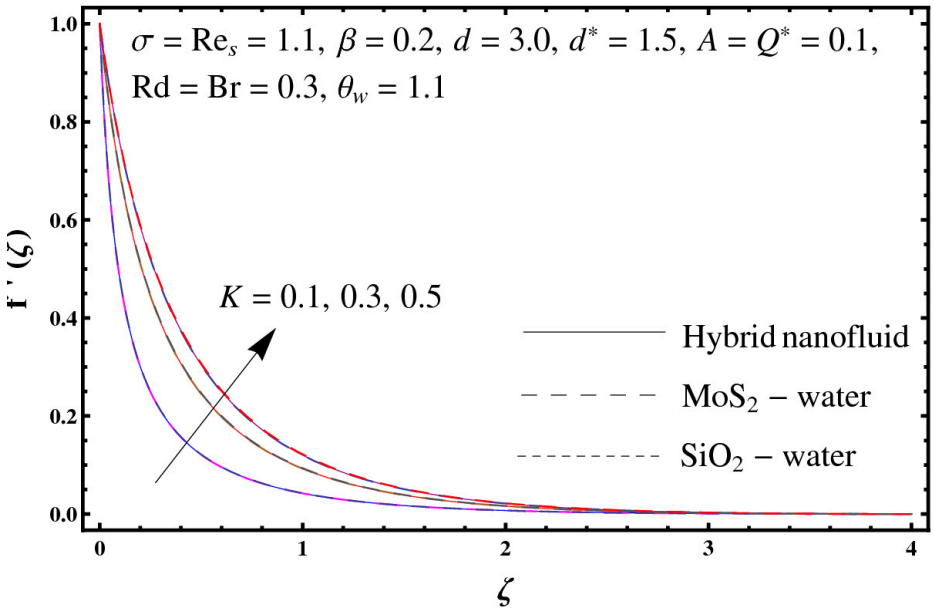

Figure 2. Sketch of $f'(\zeta)$ against K.

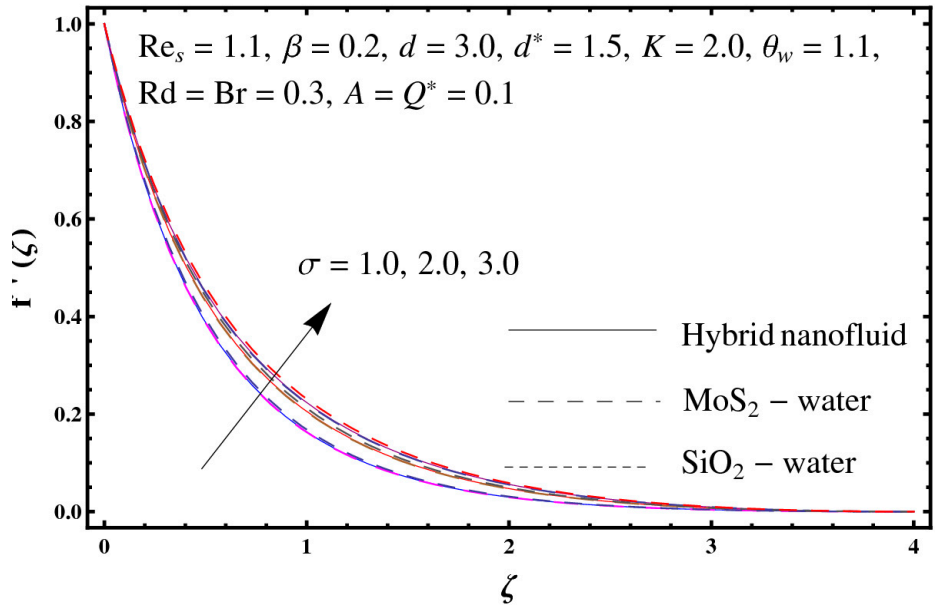

Figure 3. Sketch of $f'(\zeta)$ against σ.

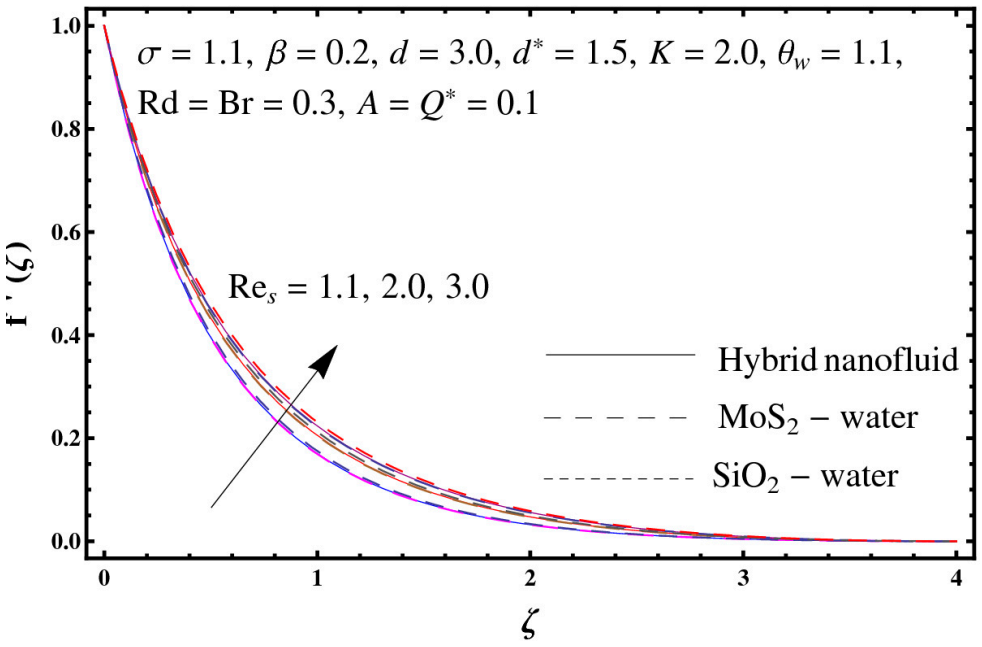

Figure 4. Sketch of $f'(\zeta)$ against Re_s.

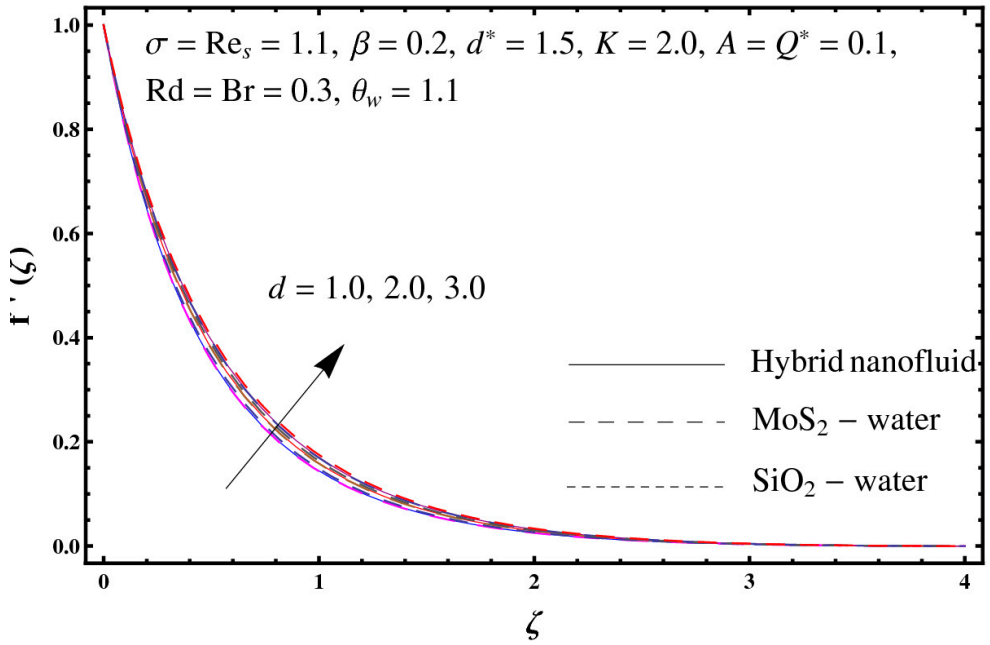

Figure 5. Sketch of $f'(\zeta)$ against d.

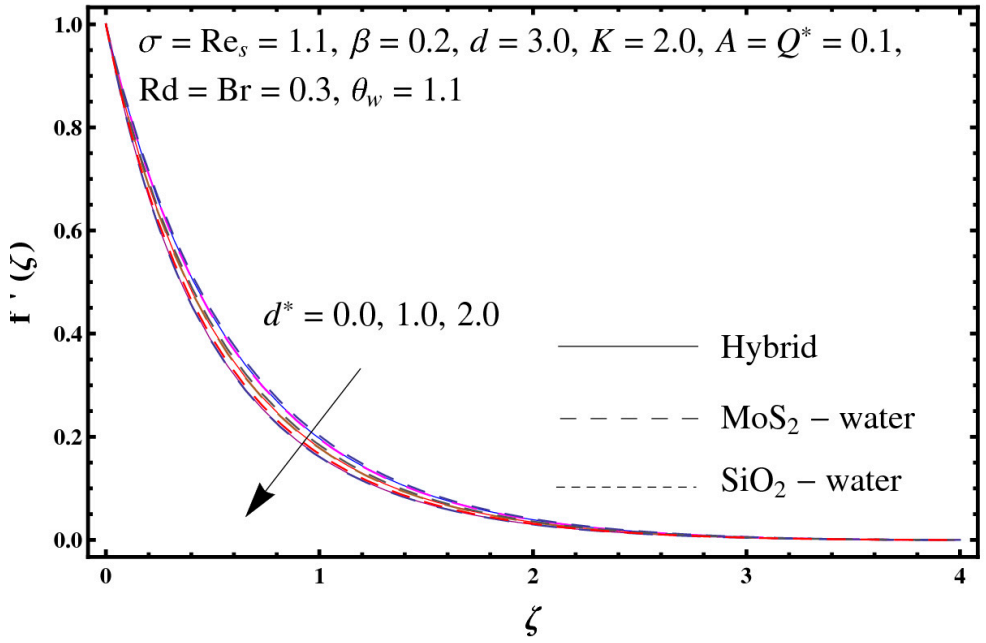

Figure 6. Sketch of $f'(\zeta)$ against d^*.

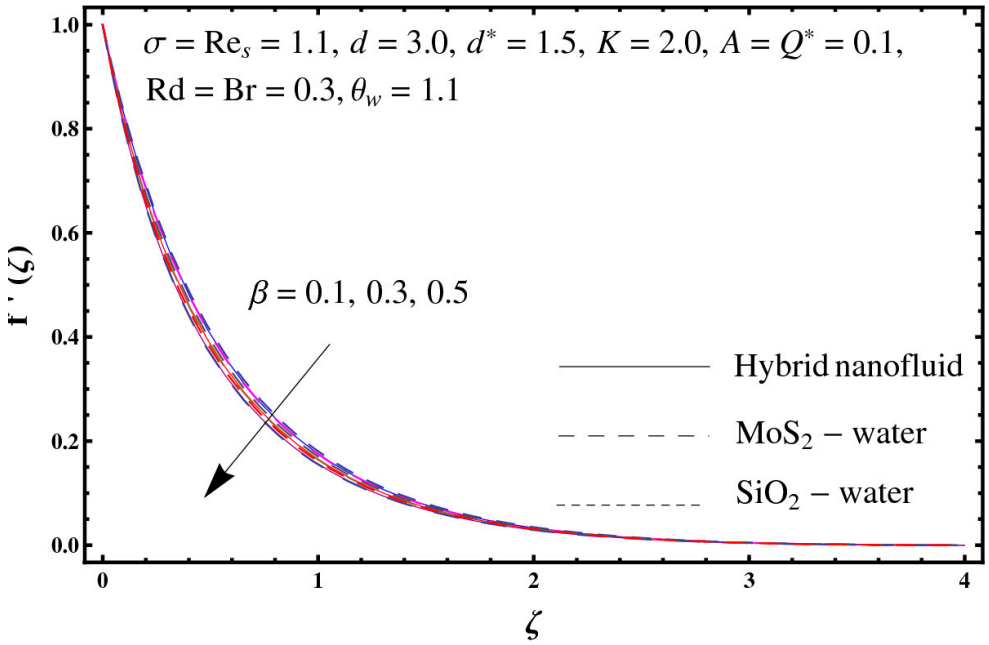

Figure 7. Sketch of $f'(\zeta)$ against β.

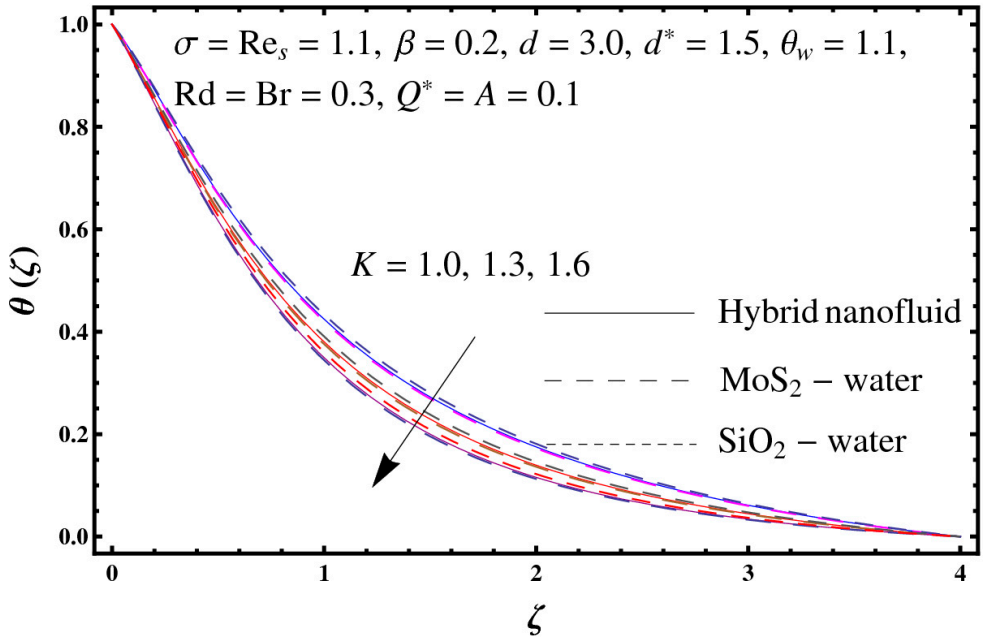

Figure 8. Sketch of $\theta(\zeta)$ against K.

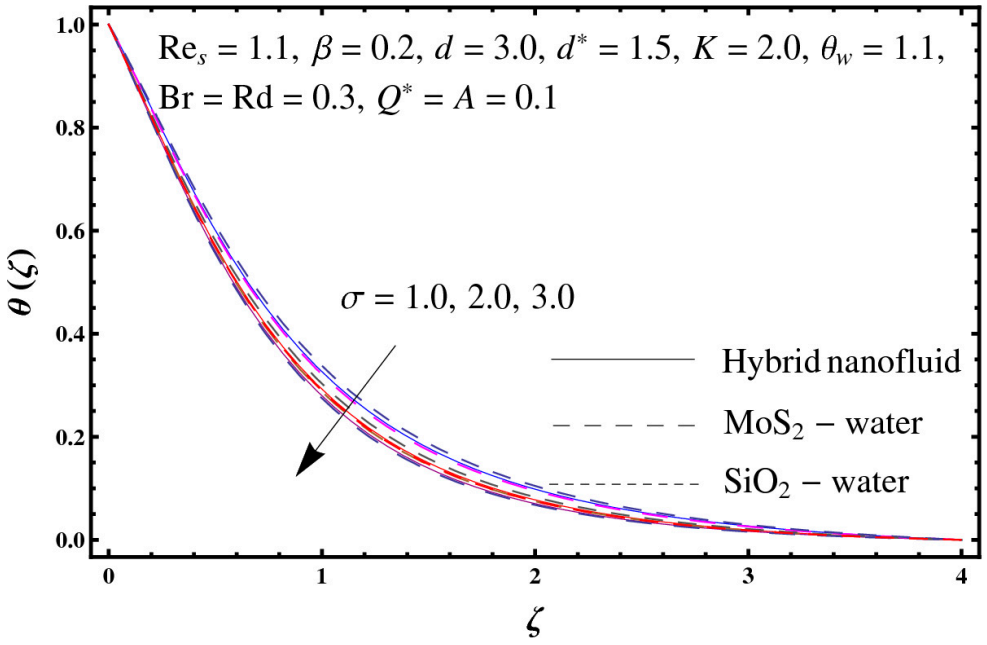

Figure 9. Sketch of $\theta(\zeta)$ against σ.

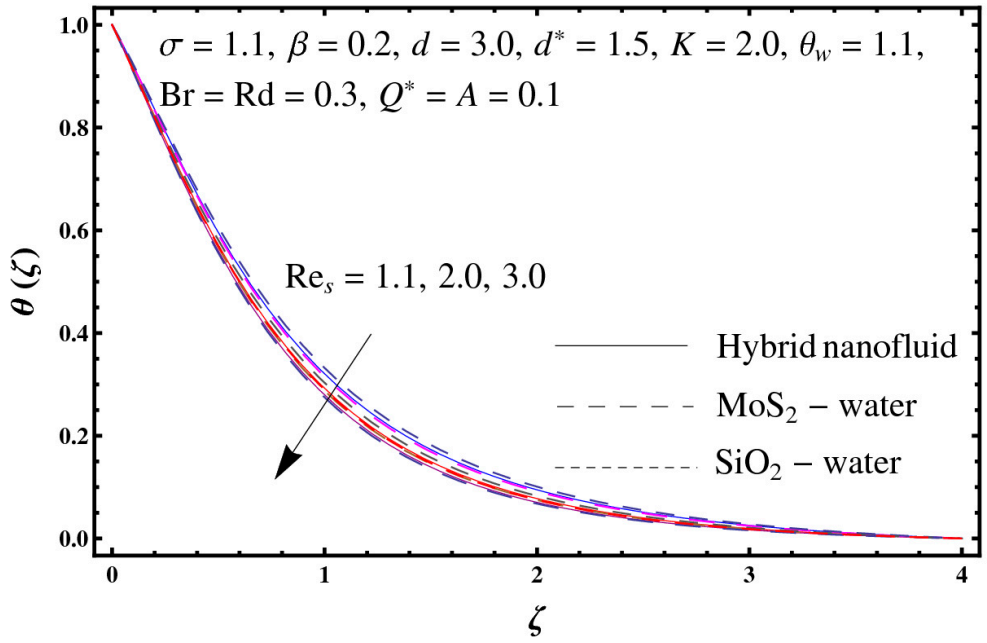

Figure 10. Sketch of $\theta(\zeta)$ against Re_s.

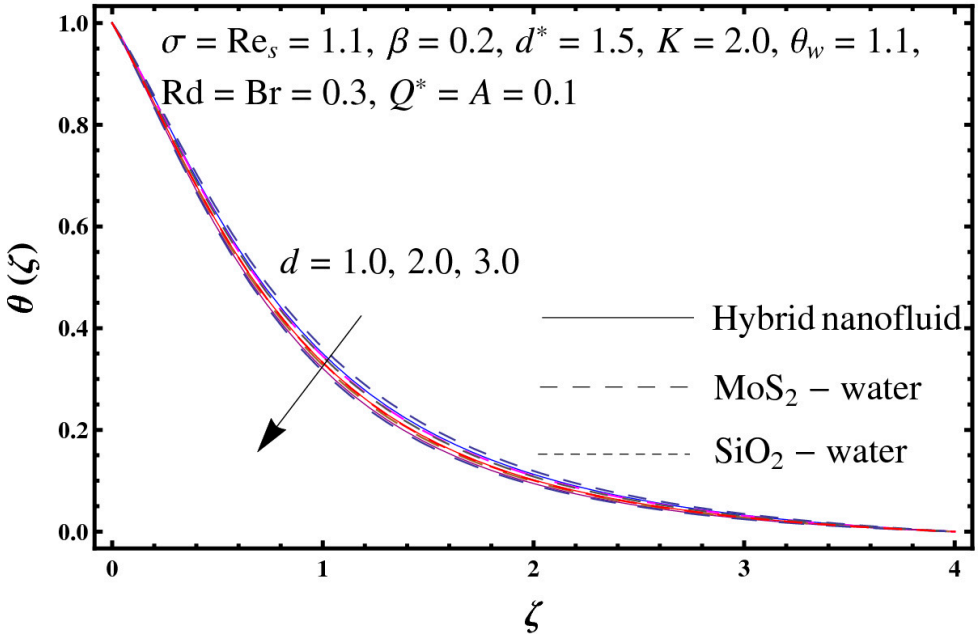

Figure 11. Sketch of $\theta(\zeta)$ against d.

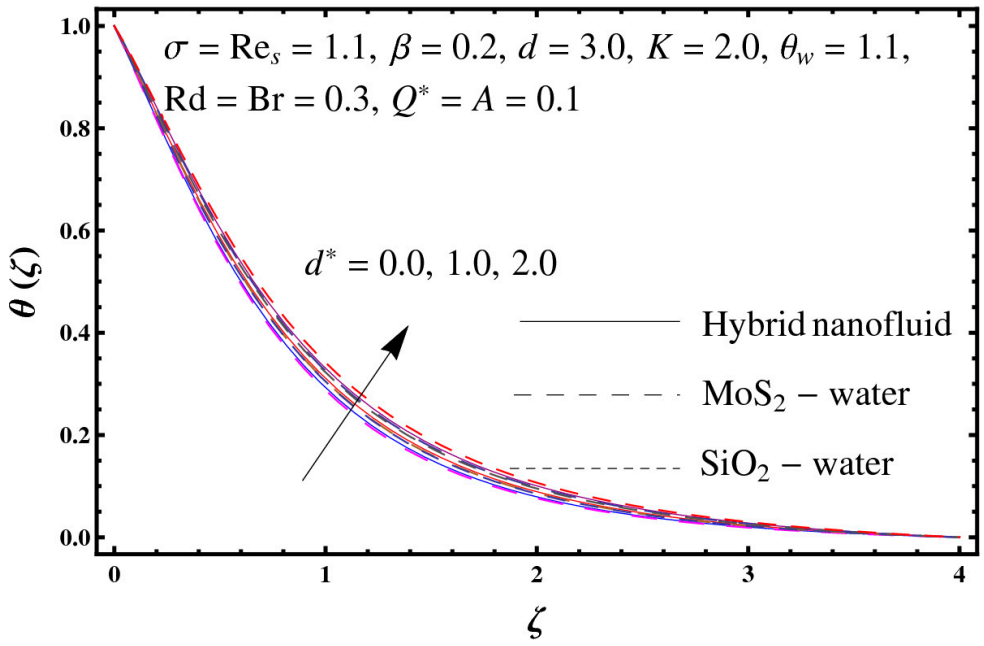

Figure 12. Sketch of $\theta(\zeta)$ against d^*.

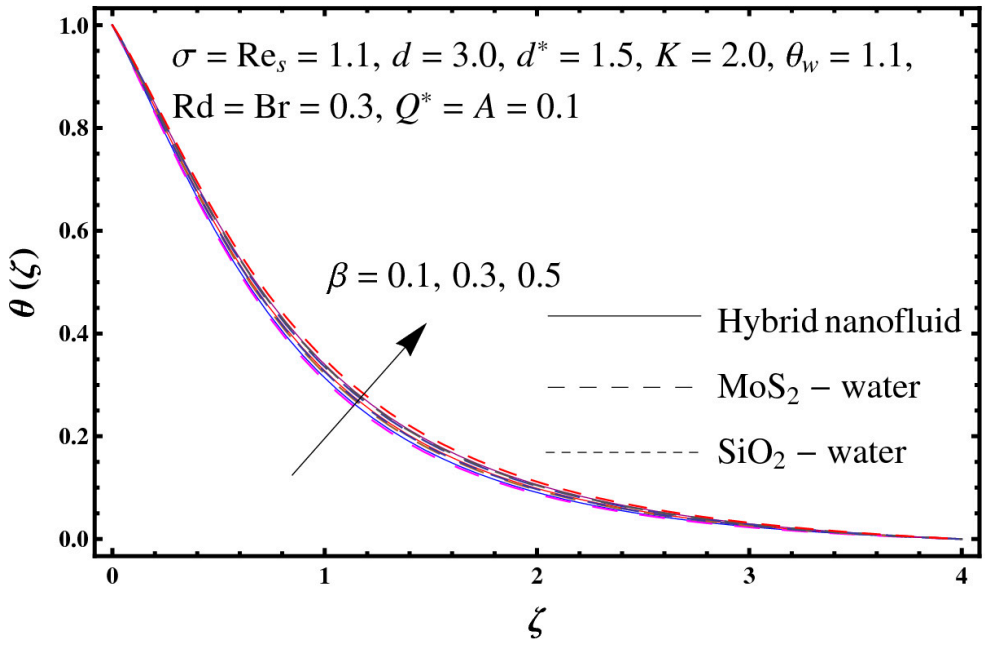

Figure 13. Sketch of $\theta(\zeta)$ against β.

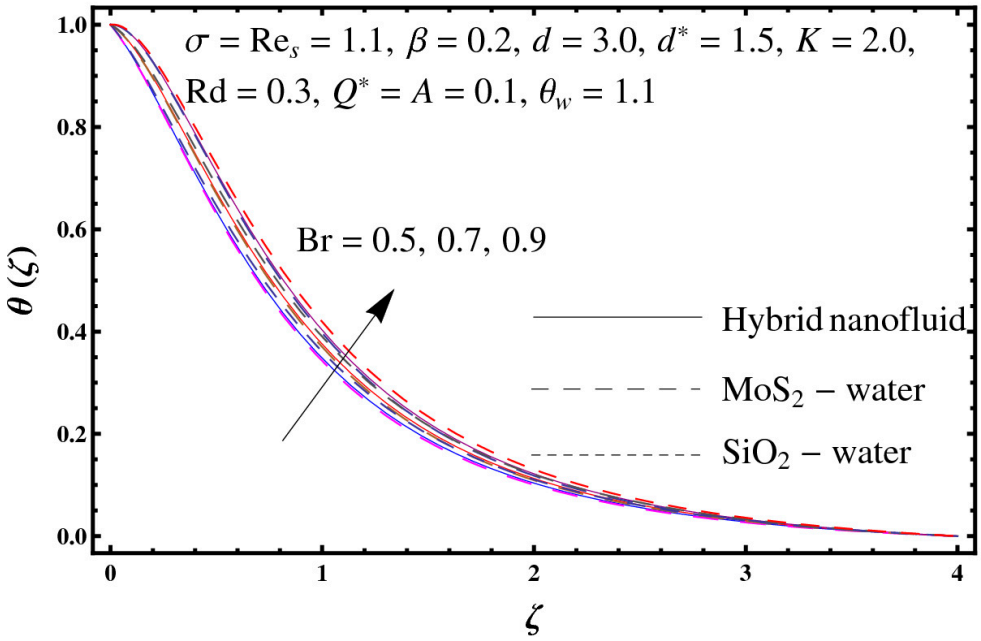

Figure 14. Sketch of $\theta(\zeta)$ against Br.

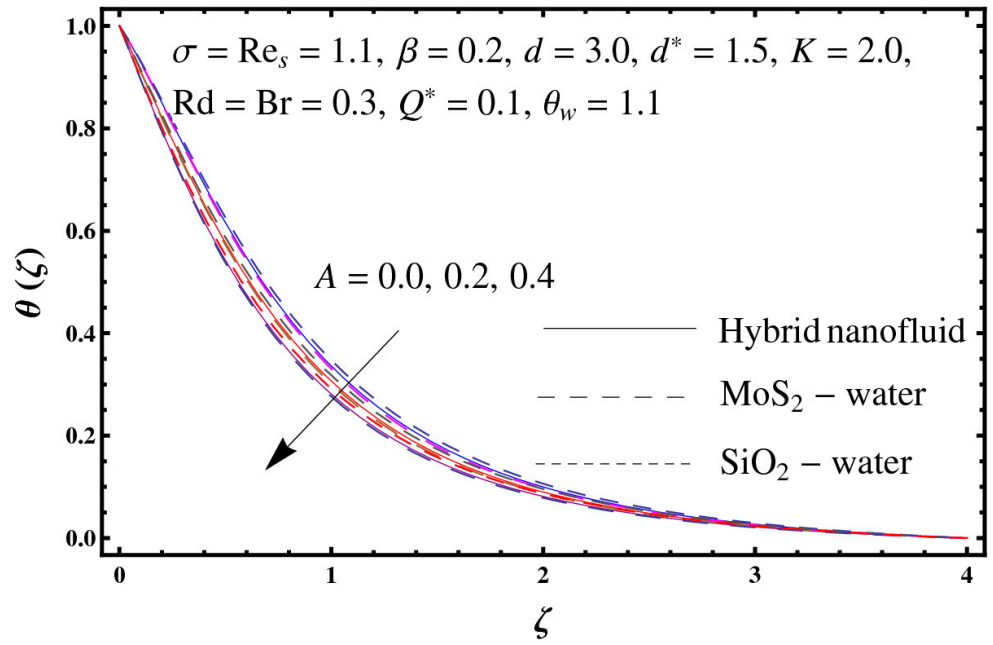

Figure 15. Sketch of $\theta(\zeta)$ against A.

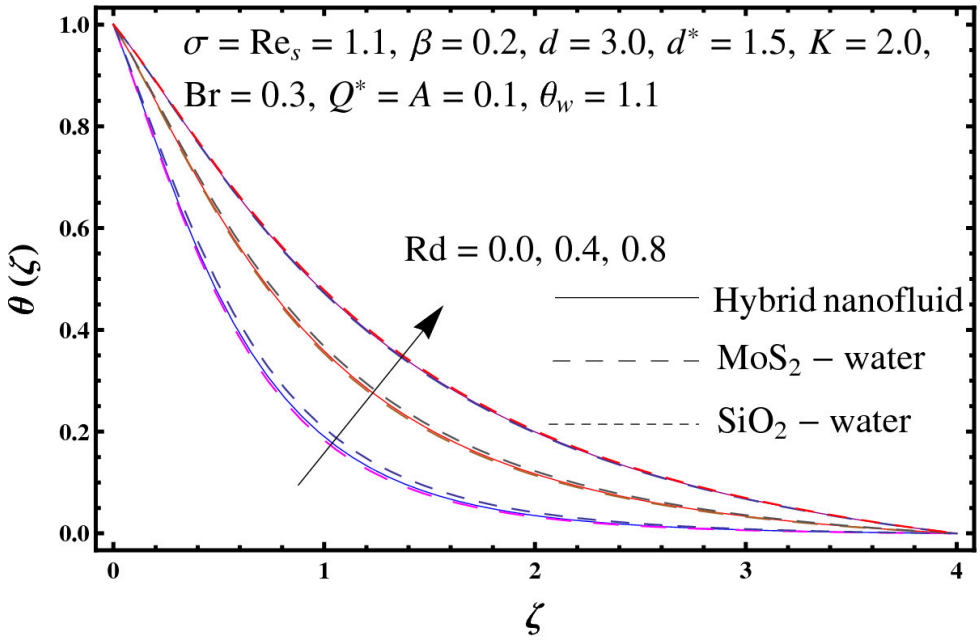

Figure 16. Sketch of $\theta(\zeta)$ against Rd.

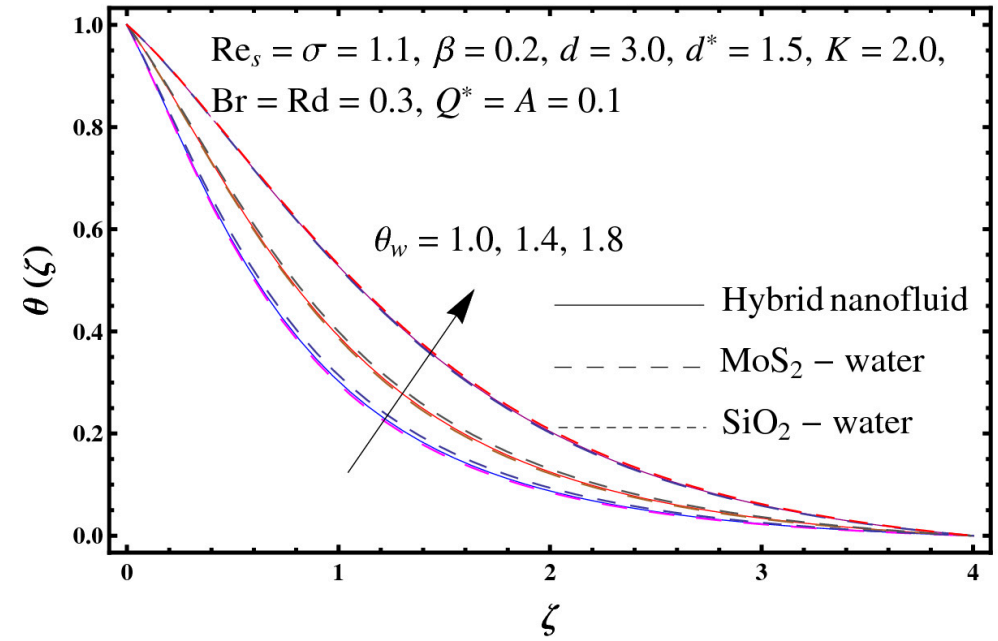

Figure 17. Sketch of $\theta(\zeta)$ against θ_w.

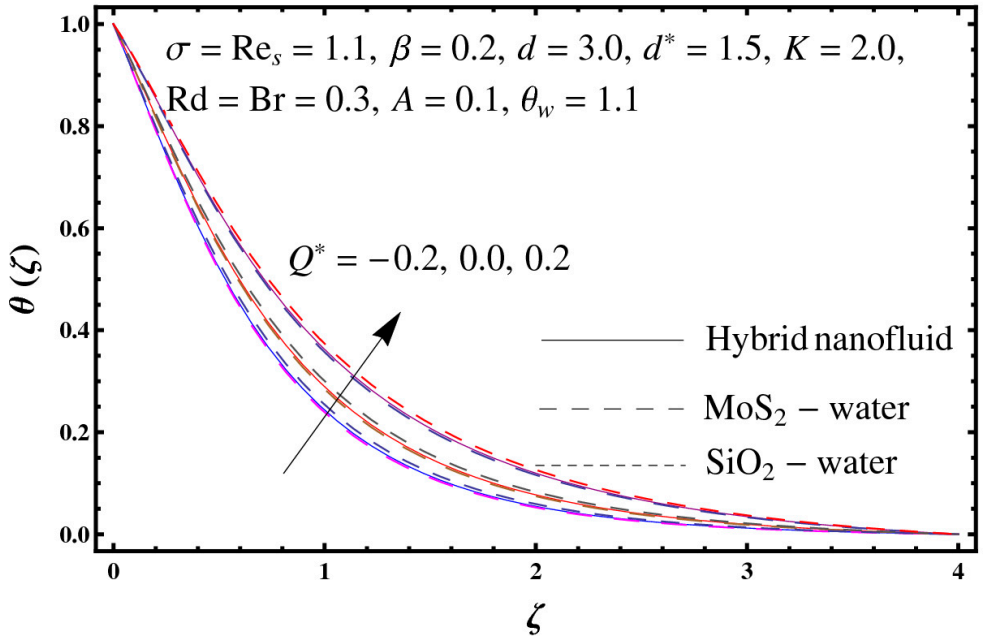

Figure 18. Sketch of $\theta(\zeta)$ against Q^*.

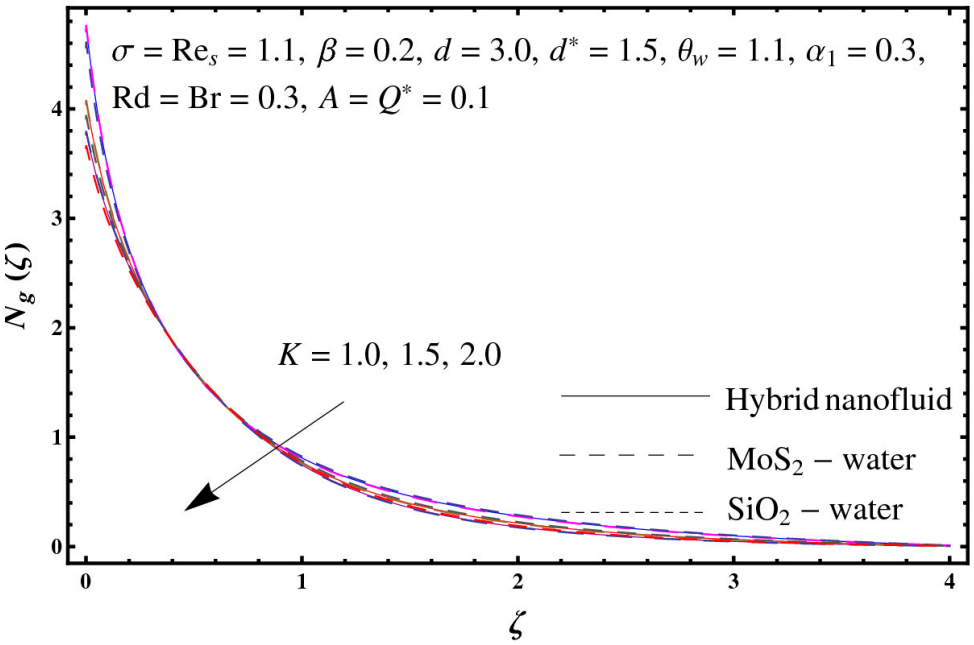

Figure 19. Sketch of $N_g(\zeta)$ against K.

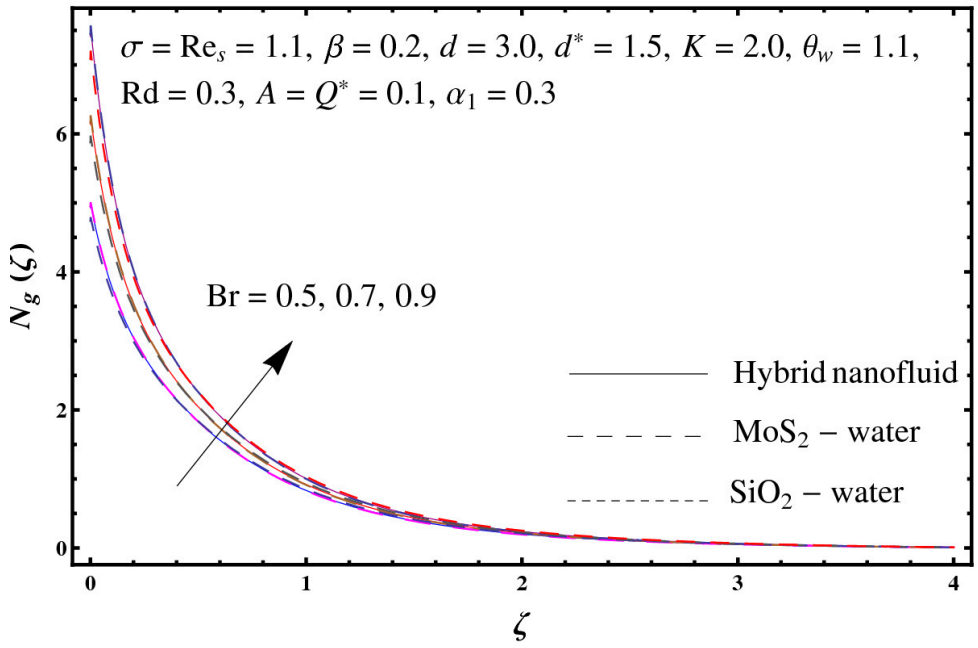

Figure 20. Sketch of $N_g(\zeta)$ against Br.

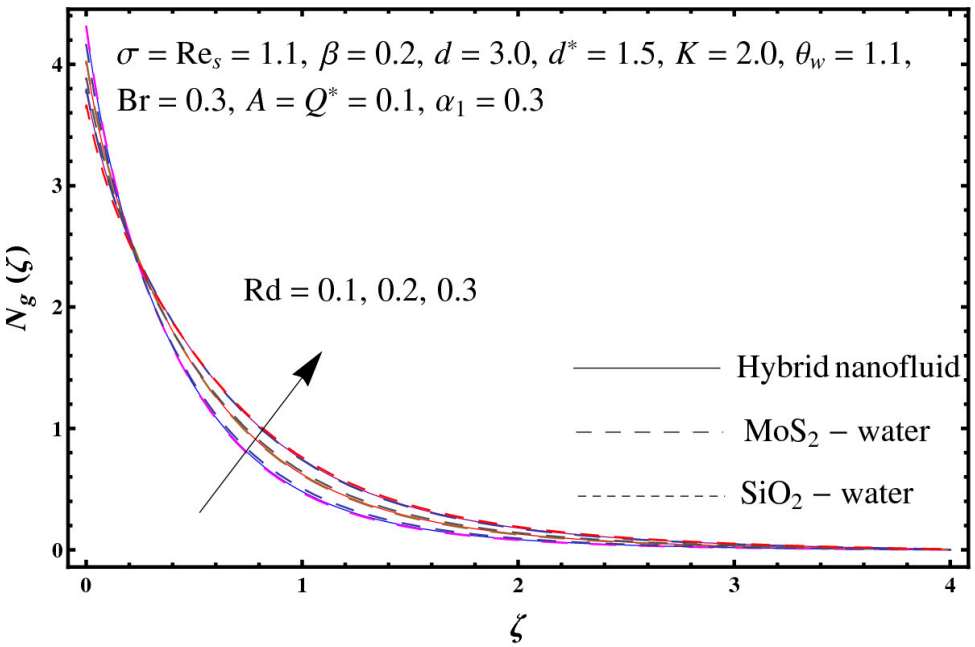

Figure 21. Sketch of $N_g(\zeta)$ against Rd.

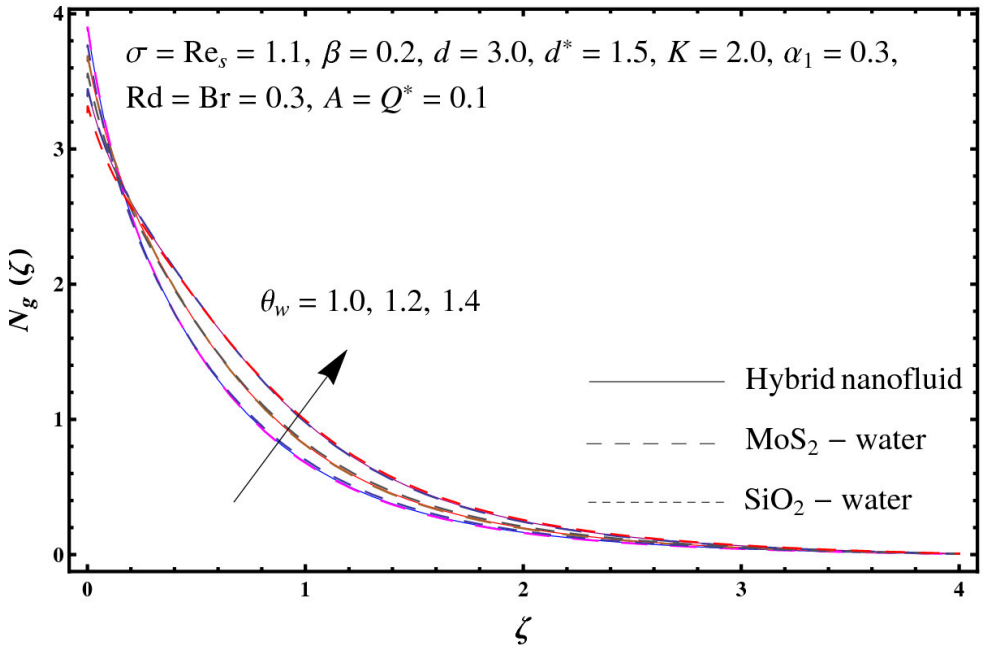

Figure 22. Sketch of $N_g(\zeta)$ against θ_w.

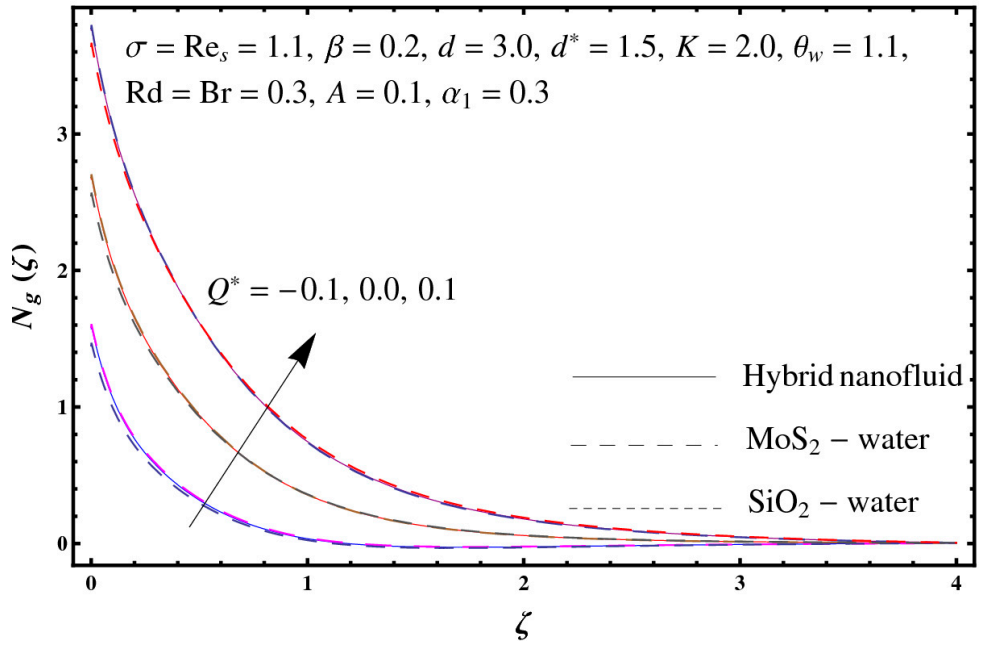

Figure 23. Sketch of $N_g(\zeta)$ against Q^*.

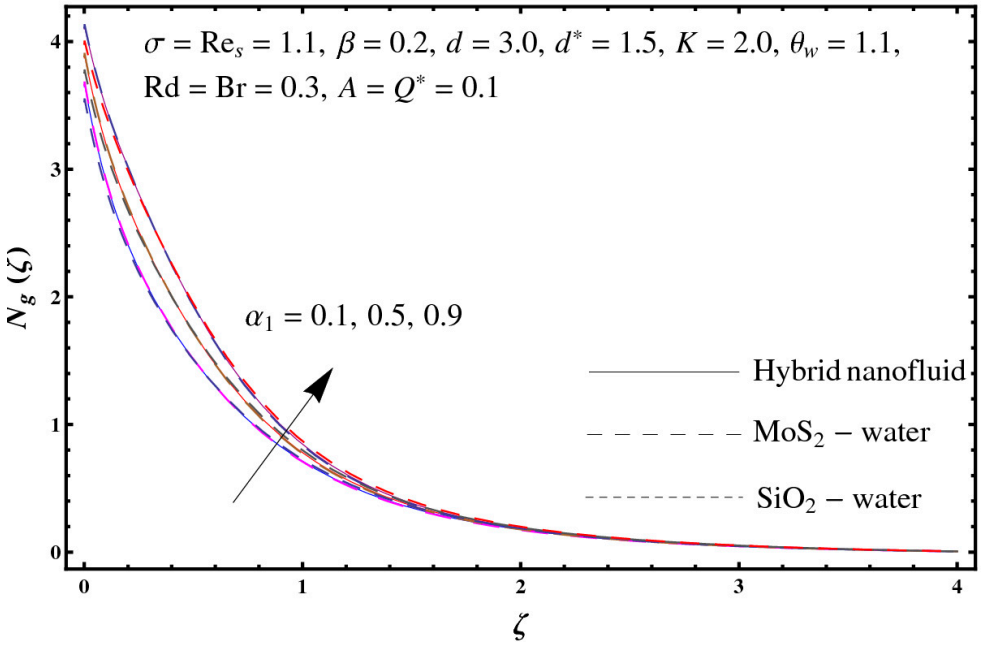

Figure 24. Sketch of $N_g(\zeta)$ against α_1.

Table 2. Numerical data of skin friction coefficient $\left(\frac{\mathrm{Re}_s}{2}\right)^{1/2} C_f$ for K, σ, Re_s, d, d^*, and β.

K	σ	Re_s	d	d^*	β	$\left(\frac{\mathrm{Re}_s}{2}\right)^{1/2} C_f$		
						Hybrid Nanofluid	**MoS_2-Water**	**SiO_2-Water**
1.0	1.1	1.1	3.0	1.5	0.2	3.84238	3.85225	3.79266
1.3						3.41971	3.43047	3.36545
1.5						3.23852	3.24971	3.18205
2.0	1.0	1.1	3.0	1.5	0.2	2.99600	3.00776	2.93661
	2.0					2.75157	2.76442	2.68650
	3.0					2.65921	2.67253	2.59173
2.0	1.1	1.1	3.0	1.5	0.2	2.95453	2.96646	2.89425
		1.5				2.83785	2.85030	2.77490
		1.9				2.76557	2.77835	2.70085
2.0	1.1	1.1	1.0	1.5	0.2	3.24720	3.25959	3.18459
			2.0			3.06787	3.07997	3.00672
			3.0			2.95453	2.96646	2.89425
2.0	1.1	1.1	3.0	0.0	0.2	2.64363	2.65338	2.59446
				1.0		2.84189	2.85292	2.78613
				2.0		3.07546	3.08842	3.00990
2.0	1.1	1.1	3.0	1.5	0.0	2.74260	2.75107	2.69994
					0.1	2.85047	2.86073	2.79873
					0.3	3.05515	3.06865	2.98681

Table 3. Numerical data of local Nusselt number $\left(\frac{\mathrm{Re}_s}{2}\right)^{-1/2} Nu$ for K, σ, Re_s, d, d^*, β, Br, Rd, θ_w and Q^*.

K	σ	Re_s	d	d^*	β	Br	Rd	θ_w	Q^*	$\left(\frac{\mathrm{Re}_s}{2}\right)^{-1/2} Nu$		
										Hybrid Nanofluid	**MoS_2-Water**	**SiO_2-Water**
1.0	1.1	1.1	3.0	1.5	0.2	0.3	0.3	1.1	0.1	0.78812	0.77888	0.78773
1.3										0.95609	0.94689	0.96164
1.6										1.06312	1.05373	1.07280
2.0	1.0	1.1	3.0	1.5	0.2	0.3	0.3	1.1	0.1	1.12722	1.11800	1.13864
	2.0									1.29904	1.28665	1.32381
	3.0									1.36435	1.35064	1.39455
2.0	1.1	1.1	3.0	1.5	0.2	0.3	0.3	1.1	0.1	1.15619	1.14646	1.16977
		2.0								1.29904	1.28665	1.32381
		3.0								1.36435	1.35064	1.39455
2.0	1.1	1.1	3.0	0.0	0.2	0.3	0.3	1.1	0.1	1.36447	1.35379	1.38047
				1.0						1.23024	1.22030	1.24414
				2.0						1.07829	1.06870	1.09196
2.0	1.1	1.1	3.0	1.5	0.0	0.3	0.3	1.1	0.1	1.28077	1.27229	1.28646
					0.1					1.21696	1.20783	1.22679
					0.3					1.09811	1.08785	1.11512
2.0	1.1	1.1	3.0	1.5	0.2	0.5	0.3	1.1	0.1	0.75746	0.75223	0.74922
						0.6				0.55799	0.55499	0.53882
						0.7				0.35843	0.35767	0.32834
2.0	1.1	1.1	3.0	1.5	0.2	0.3	0.0	1.1	0.1	1.09425	1.08172	1.11263
							0.4			1.16916	1.15964	1.18257
							0.8			1.22079	1.21096	1.23532
2.0	1.1	1.1	3.0	1.5	0.2	0.3	0.3	1.0	0.1	1.14395	1.13379	1.15834
								1.4		1.18662	1.17787	1.19835
								1.8		1.19871	1.19025	1.21112
2.0	1.1	1.1	3.0	1.5	0.2	0.3	0.3	1.1	−0.2	1.55119	1.53599	1.57635
									0.0	1.30480	1.29301	1.32259
									0.2	0.97895	0.97161	0.98815

Table 4. Comparative values of skin friction coefficient $\left(\frac{\mathrm{Re}_s}{2}\right)^{1/2} C_f$ for distinct values of K.

K	$-\left(\frac{\mathrm{Re}_s}{2}\right)^{1/2} C_f$	
	Okechi et al. [28]	**Present**
5	1.4196	1.45703
10	1.3467	1.36819
20	1.3135	1.32810
30	1.3028	1.31536
40	1.2975	1.30912
50	1.2944	1.30539
100	1.2881	1.29804
200	1.2850	1.29443
1000	1.2826	1.29152

6. Conclusions

The main points of the current analysis are:

- Velocity has the opposite scenario for variable characteristics of porosity and permeability.
- Aspects of the permeability parameter on velocity are reversed when compared with the thermal field.
- Enhancement in velocity is witnessed against the curvature parameter.
- Temperature against Brinkman number and radiation parameter have a similar trend.
- Augmentation in the thermal field is observed through the inertia coefficient.
- Entropy generation rate increases for heat generation/absorption and temperature ratio parameter.
- Skin friction coefficient for variable permeability parameter decays.
- Augmentation in local Nusselt number is witnessed for radiation and temperature ratio parameters.
- Some possible extension of the current analysis may be as follows:
- Importance of melting heat transfer effects inflow of hybrid nanofluid.
- Binary chemical reaction and activation energy aspects inflow by curved stretching surface.
- Modeling of non-Newtonian liquids inflow due to curved geometry.

Author Contributions: M.A.S., F.H. and T.H. contributed in mathematical modeling, computation of numerical solutions, analysis of results and writing of article. All authors have read and agreed to the published version of the manuscript.

Funding: This research was funded by KFUPM, grant number SB191015.

Institutional Review Board Statement: Not applicable.

Informed Consent Statement: Not applicable.

Data Availability Statement: Data is contained within the article.

Acknowledgments: We wish to express our thanks for the financial support of this research from King Fahd University of Petroleum and Minerals.

Conflicts of Interest: The authors declare no conflict of interest.

Abbreviations

R	Radius of curvature	s, r	space coordinate
u, v	velocity components	U_w	surface stretching velocity
ρ_1, ρ_2	densities of nanaparticles	μ_f	fluid dynamic viscosity
d	variable permeability	k_1, k_2	thermal conductivity of nanoparticle
ρ_f	fluid density	d^*	variable porosity
ν_f	kinematic fluid viscosity	ν_{hnf}	kinematic viscosity of hybrid nanofluid
k_f	basefluid thermal conductivity	k_{hnf}	thermal conductivity of hybrid nanofluid
α_f	thermal diffusivity of base fluid	T_w	surface temperature
α_{hnf}	thermal diffusivity of hybrid nanofluid	T_∞	ambient temperature
ε	porosity	k^*	permeability of porous medium
p	pressure	C_b	drag coefficient
Q	heat generation/absorption	$\widetilde{\sigma}$	Stefan Boltzmann constant
k	mean absorption coefficient	Q^*	heat generation/absorption parameter
F	non-uniform inertia coefficient	ϕ_1, ϕ_2	solid volume fraction of nanoparticles
Rd	radiation parameter	Re_s	local Reynolds number
β	Inertia coefficient	Br	Brinkman number
C_f	skin friction coefficient	Nu_s	local Nusselt number
σ	local porosity parameter	Pe_s	Peclet number
θ	dimensionless temperature	f'	dimensionless velocity
K	curvature parameter	$N_g(\zeta)$	entropy generation rate
H	dimensionless pressure	ζ	dimensionless variable
Pr	Prandtl number	A	temperature exponent

References

1. Choi, S.U.S. *Enhancing Thermal Conductivity of Fluids with Nanoparticles*; Argonne National Lab.: DuPage County, IL, USA, 1995; Volume 66, pp. 99–105.
2. Eastman, J.A.; Choi, S.U.S.; Li, S.; Yu, W.; Thompson, L.J. Anomalously increased effective thermal conductivity of ethylene glycol-based nanofluids containing copper nanoparticles. *Appl. Phys. Lett.* **2001**, *78*, 718–720. [CrossRef]
3. Tiwari, R.K.; Das, M.K. Heat transfer augmentation in a two-sided lid-driven differentially heated square cavity utilizing nanofluid. *Int. J. Heat Mass Transf.* **2007**, *50*, 2002–2018. [CrossRef]
4. Vajravelu, K.; Prasad, K.V.; Lee, J.; Lee, C.; Pop, I.; Gorder, R.A.V. Convective heat transfer in the flow of viscous Ag-water and Cu-water nanofluids over a stretching surface. *Int. J. Therm. Sci.* **2011**, *50*, 843–851. [CrossRef]
5. Khan, J.A.; Mustafa, M.; Hayat, T.; Farooq, M.A.; Alsaedi, A.; Liao, S.J. On model for three-dimensional flow of nanofluid: An application to solar energy. *J. Mol. Liq.* **2014**, *194*, 41–47. [CrossRef]
6. Devasenan, M.; Kalaiselvam, S. Experimental analysis of hybrid nanofluid as a coolant. *Procedia Eng.* **2014**, *97*, 1667–1675.
7. Malvandi, A.; Safaei, M.R.; Kaffash, M.H.; Ganji, D.D. MHD mixed convection in a vertical annulus filled with Al_2O_3-water nanofluid considering nanoparticle migration. *J. Magn. Magn. Mater.* **2015**, *382*, 296–306. [CrossRef]
8. Selimefendigil, F.; Öztop, H.F.; Abu-Hamdeh, N. Mixed convection due to rotating cylinder in an internally heated and flexible walled cavity filled with SiO2-water nanofluids: Effect of nanoparticle shape. *Int. Commun. Heat Mass Transf.* **2016**, *71*, 9–19. [CrossRef]
9. Hayat, T.; Nadeem, S. Heat transfer enhancement with Ag-CuO/water hybrid nanofluid. *Results Phys.* **2017**, *7*, 2317–2324. [CrossRef]
10. Iqbal, Z.; Maraj, E.N.; Azhar, E.; Mehmood, Z. A novel development of (MoS_2-SiO_2/H_2O) hybrid nanofluidic curvilinear transport and consequences for effectiveness of shape factors. *J. Taiwan Inst. Chem. Eng.* **2017**, *81*, 150–158. [CrossRef]
11. Usman, M.; Hamid, M.; Zubair, T.; Haq, R.U.; Wang, W. Cu- Al_2O_3/water hybrid nanofluid through a permeable surface in the presence of nonlinear radiation and variable thermal conductivity via LSM. *Int. J. Heat Mass Transf.* **2018**, *126*, 1347–1356. [CrossRef]
12. Mansour, M.A.; Siddiqa, S.; Gorla, R.S.R.; Rashad, A.M. Effects of heat source and sink on entropy generation and MHD natural convection of Al_2O_3-Cu/water hybrid nanofluid filled with square porous cavity. *Therm. Sci. Eng. Prog.* **2018**, *6*, 57–71. [CrossRef]
13. Shaiq, S.; Maraj, E.N.; Iqbal, Z. Remarkable role of $C_3H_8O_2$ on transportation of MoS_2-SiO_2 hybrid nanoparticles influenced by thermal deposition and internal heat generation. *J. Phys. Chem. Solids* **2019**, *126*, 294–303. [CrossRef]
14. Khan, M.I.; Khan, S.A.; Hayat, T.; Waqas, M.; Alsaedi, A. Modeling and numerical simulation for flow of hybrid nanofluid (SiO_2/$C_3H_8O_2$) and (MoS_2/$C_3H_8O_2$) with entropy optimization and variable viscosity. *Int. J. Numer. Heat Fluid Flow* **2019**, *30*, 3939–3955. [CrossRef]
15. Iqbal, M.S.; Mustafa, I.; Ghaffari, A. Analysis of heat transfer enrichment in hydromagnetic flow of hybrid nanofluid along vertical wavy surface. *J. Magn.* **2019**, *24*, 271–280. [CrossRef]

16. Khan, S.A.; Khan, M.I.; Hayat, T.; Alsaedi, A. Darcy-Forchheimer hybrid (MoS_2, SiO_2) nanofluid flow with entropy generation. *Comput. Meth. Prog. Biomed.* **2020**, *185*, 105152. [CrossRef]
17. Acharya, N. On the flow patterns and thermal behaviour of hybrid nanofluid flow inside a microchannel in presence of radiative solar energy. *J. Therm. Anal. Calorim.* **2020**, *141*, 1425–1442. [CrossRef]
18. Aladdin, N.A.L.; Bachok, N.; Pop, I. Cu-Al_2O_3/water hybrid nanofluid flow over a permeable moving surface in presence of hydromagnetic and suction effects. *Alex. Eng. J.* **2020**, *59*, 657–666. [CrossRef]
19. Waini, I.; Ishak, A.; Groşan, T.; Pop, I. Mixed convection of a hybrid nanofluid flow along a vertical surface embedded in a porous medium. *Int. Commun. Heat Mass Transf.* **2020**, *114*, 104565. [CrossRef]
20. Aly, E.H.; Pop, I. MHD flow and heat transfer near stagnation point over a stretching/shrinking surface with partial slip and viscous dissipation: Hybrid nanofluid versus nanofluid. *Powder Technol.* **2020**, *3671*, 192–205. [CrossRef]
21. Forchheimer, P. Wasserbewegung durch boden. *Z. Ver. Dtsch. Ing.* **1901**, *45*, 1782–1788.
22. Brinkman, H.C. A calculation of the viscous force exerted by a flowing fluid on a dense swarm of particles. *Appl. Sci. Res.* **1947**, *1*, 27–34. [CrossRef]
23. Brinkman, H.C. On the permeability of media consisting of closely packed porous particles. *Appl. Sci. Res.* **1947**, *1*, 81–86. [CrossRef]
24. Nield, D.A. Resolution of a paradox involving viscous dissipation and nonlinear drag in a porous medium. *Transp. Porous Med.* **2000**, *41*, 349–357. [CrossRef]
25. Al-Hadhrami, A.K.; Elliott, L.; Ingham, D.B. A new model for viscous dissipation in porous media across a range of permeability values. *Trans. Porous Med.* **2003**, *53*, 17–122. [CrossRef]
26. Seddeek, M.A. Influence of viscous dissipation and thermophoresis on Darcy-Forchheimer mixed convection in a fluid saturated porous media. *J. Colloid Interface Sci.* **2006**, *293*, 137–142. [CrossRef]
27. Umavathi, J.C.; Ojjela, O.; Vajravelu, K. Numerical analysis of natural convective flow and heat transfer of nanofluids in a vertical rectangular duct using Darcy-Forchheimer-Brinkman model. *Int. J. Therm. Sci.* **2017**, *111*, 511–524. [CrossRef]
28. Okechi, N.F.; Jalil, M.; Asghar, S. Flow of viscous fluid along an exponentially stretching curved surface. *Results Phys.* **2017**, *7*, 2851–2854. [CrossRef]
29. Bhatti, M.M.; Zeeshan, A.; Ellahi, R.; Shit, G.C. Mathematical modeling of heat and mass transfer effects on MHD peristaltic propulsion of two-phase flow through a Darcy-Brinkman-Forchheimer porous medium. *Adv. Powder Tech.* **2018**, *29*, 1189–1197. [CrossRef]
30. Shashikumar, N.S.; Gireesha, B.J.; Mahanthesh, B.; Prasannakumara, B.C. Brinkman-Forchheimer flow of SWCNT and MWCNT magneto-nanoliquids in a microchannel with multiple slips and Joule heating aspects. *Multidiscip. Model. Mater. Struct.* **2018**, *14*, 769–786.
31. Shao, Q.; Fahs, M.; Hoteit, H.; Carrera, J.; Ackerer, P.; Younes, A. A 3D semi-analytical solution for density-driven flow in porous media. *Water Resour. Res.* **2018**, *54*, 10094–10116. [CrossRef]
32. Rasool, G.; Zhang, T.; Chamkha, A.J.; Shafiq, A.; Tlili, I.; Shahzadi, G. Entropy generation and consequences of binary chemical reaction on MHD Darcy-Forchheimer Williamson nanofluid flow over non-linearly stretching surface. *Entropy* **2020**, *22*, 18. [CrossRef] [PubMed]
33. Tlili, I.; Ramzan, M.; Kadry, S.; Kim, H.-W.; Nam, Y. Radiative MHD nanofluid flow over a moving thin needle with entropy generation in a porous medium with dust particles and Hall current. *Entropy* **2020**, *22*, 354. [CrossRef] [PubMed]
34. Fahs, M.; Graf, T.; Tran, T.V.; Ataie-Ashtiani, B.; Simmons, C.T.; Younes, A. Study of the effect of thermal dispersion on internal natural convection in porous media using Fourier series. *Transp. Porous Med.* **2020**, *131*, 537–568. [CrossRef]
35. Aminian, E.; Moghadasi, H.; Saffari, H.; Gheitaghy, A.M. Investigation of forced convection enhancement and entropy generation of nanofluid flow through a corrugated minichannel filled with a porous media. *Entropy* **2020**, *22*, 1008. [CrossRef]
36. Muhammad, T.; Rafique, K.; Asma, M.; Alghamdi, M. Darcy-Forchheimer flow over an exponentially stretching curved surface with Cattaneo-Christov double diffusion. *Physica A* **2020**, *556*, 123968. [CrossRef]
37. Vafai, K. Convective flow and heat transfer in variable porosity media. *J. Fluid Mech.* **1984**, *147*, 233–259. [CrossRef]
38. Vafai, K.; Alkire, R.L.; Tien, C.L. An experimental investigation of heat transfer in variable porosity media. *J. Heat Transf.* **1985**, *107*, 642–947. [CrossRef]
39. Chandrasekhara, B.C.; Namboudiri, P.M.S. Influence of variable permeability on combined free and forced convection about inclined surfaces in porous media. *Int. J. Heat Mass Transf.* **1985**, *28*, 199–206. [CrossRef]
40. Ibrahim, F.S.; Hassanien, I.A. Influence of variable permeability on combined convection along a nonisothermal wedge in a saturated porous medium. *Transp. Porous Med.* **2000**, *39*, 57–71. [CrossRef]
41. Rees, D.A.S.; Pop, I. Vertical free convection in a porous medium with variable permeability effects. *Int. J. Heat Mass Transf.* **2000**, *43*, 2565–2571. [CrossRef]
42. Hamdan, M.H.; Kamel, M.T. Flow through variable permeability porous layers. *Adv. Theor. Appl. Mech.* **2011**, *4*, 135–145.
43. Saif, R.S.; Muhammad, T.; Sadia, H. Significance of inclined magnetic field in Darcy-Forchheimer flow with variable porosity and thermal conductivity. *Physica A* **2020**, *551*, 124067. [CrossRef]
44. Jing, D.; Song, J.; Sui, Y. Hydraulic and thermal performances of laminar flow in fractal treelike branching microchannel network with wall velocity slip. *Fractals* **2020**, *28*, 2050022. [CrossRef]
45. Bejan, A. A study of entropy generation in fundamental convective heat transfer. *J. Heat Transf.* **1979**, *101*, 718–725. [CrossRef]

46. Mahmoudi, A.; Mejri, I.; Abbassi, M.A.; Omri, A. Analysis of the entropy generation in a nanofluid-filled cavity in the presence of magnetic field and uniform heat generation/absorption. *J. Mol. Liq.* **2014**, *198*, 63–77. [CrossRef]
47. López, A.; Ibáñez, G.; Pantoja, J.; Moreira, J.; Lastres, O. Entropy generation analysis of MHD nanofluid flow in a porous vertical microchannel with nonlinear thermal radiation, slip flow and convective-radiative boundary conditions. *Int. J. Heat Mass Transf.* **2017**, *107*, 982–994. [CrossRef]
48. Sithole, H.; Mondal, H.; Sibanda, P. Entropy generation in a second grade magnetohydrodynamic nanofluid flow over a convectively heated stretching sheet with nonlinear thermal radiation and viscous dissipation. *Results Phys.* **2018**, *9*, 1077–1085. [CrossRef]
49. Astanina, M.S.; Sheremet, M.A.; Oztop, H.F.; Abu-Hamdeh, N. MHD natural convection and entropy generation of ferrofluid in an open trapezoidal cavity partially filled with a porous medium. *Int. J. Mech. Sci.* **2018**, *136*, 493–502. [CrossRef]
50. Huminic, G.; Huminic, A. The heat transfer performances and entropy generation analysis of hybrid nanofluids in a flattened tube. *Int. J. Heat Mass Transf.* **2018**, *119*, 813–827. [CrossRef]
51. Ganesh, N.V.; Al-Mdallal, Q.M.; Chamkha, A.J. A numerical investigation of Newtonian fluid flow with buoyancy, thermal slip of order two and entropy generation. *Case Stud. Therm. Eng.* **2019**, *13*, 100376. [CrossRef]
52. Kashyap, D.; Dass, A.K. Effect of boundary conditions on heat transfer and entropy generation during two-phase mixed convection hybrid Al_2O_3-Cu/water nanofluid flow in a cavity. *Int. J. Mech. Sci.* **2019**, *157–158*, 45–59. [CrossRef]
53. Sheikholeslami, M.; Arabkoohsar, A.; Ismail, K.A.R. Entropy analysis for a nanofluid within a porous media with magnetic force impact using non-Darcy model. *Int. Commun. Heat Mass Transf.* **2020**, *112*, 104488. [CrossRef]
54. Muhammad, R.; Khan, M.I.; Jameel, M.; Khan, N.B. Fully developed Darcy-Forchheimer mixed convective flow over a curved surface with activation energy and entropy generation. *Comput. Meth. Prog. Biomed.* **2020**, *188*, 105298. [CrossRef] [PubMed]
55. Hayat, T.; Qayyum, S.; Alsaedi, A.; Ahmad, B. Entropy generation minimization: Darcy-Forchheimer nanofluid flow due to curved stretching sheet with partial slip. *Int. Commun. Heat Mass Transf.* **2020**, *111*, 104445. [CrossRef]
56. Hayat, T.; Shah, F.; Alsaedi, A.; Ahmad, B. Entropy optimized dissipative flow of effective Prandtl number with melting heat transport and Joule heating. *Int. Commun. Heat Mass Transf.* **2020**, *111*, 104454. [CrossRef]